Effect of collisions with a second fluid on the temporal development of nonlinear, single-mode, Rayleigh-Taylor instability

Q. Cauvet ®,* B. Bernecker ®,† S. Bouquet ®,‡ B. Canaud,§ F. Hermeline ®, and S. Pichon

CEA, DAM, DIF, 91297 Arpajon, France

Goncharov's [Phys. Rev. Lett. **88**, 134502 (2002)] nonlinear model of a single-mode Rayleigh-Taylor instability (RTI) is investigated for a partially ionized plasma in a predominantly neutral background. Terminal bubble and spike velocities are derived from the nonlinear equations in the case where the RTI dynamics is dominated by collisions between neutrals and ions. Direct numerical simulations are used to justify the use of Goncharov's model in this regime and observe its limitations.

I. INTRODUCTION

The Rayleigh-Taylor instability (RTI) occurring at the interface between two fluids subject to an external force pointing from heavy to light fluid is widely encountered in plasma physics, playing an important role in inertial confinement fusion, astrophysics, geophysics, [1–3], etc.

The linear regime of the magnetized RTI has been extensively studied through the years in either the incompressible or compressible case [4,5] or even partially ionized geophysical [6,7] or astrophysical plasmas [8,9]. For the nonlinear regime, the potential flow approach pioneered by Layzer [10] has been one of the main ways to study the classical RTI for a single-mode perturbation. People have applied this approximation to the vacuum case [11,12] and then extended it to arbitrary density ratio (see Goncharov's model [13], Sohn's model [14], Abarzhi's model [15], and Zhang's model [16]) to obtain the bubble nonlinear growth rate and curvature. More exotic methods have also been developed by the community, such as Zufiria's model [17] for the bubble and Clavin and Williams model [18] for the spikes.

RTI processes are responsible for the occurrence of some ionospheric perturbations like equatorial spread *F* (ESF). ESFs provoke disturbances of satellites and radio telecommunications near the equator, so that they have been extensively studied [3,19] since their first observation through frequency spreading on ionograms [20]. The ESF results from the rise of a so-called equatorial plasma bubble (EPB), which is a plasma bubble rising to the upper ionosphere due to a RTI process.

Another interchange instability, similar to RTI, contributes to EPB rising: the gradient drift instability (GDI) [21–23]. The difference compared to the RTI process is that the acceleration field for GDI comes from the friction between neutrals and ions and not gravity. Since both instabilities have their importance during EPB rising, they are taken conjointly under the appellation generalized Rayleigh-Taylor instability (GRTI) in our work. The particularity of ionospheric dynamics is that the plasma is only weakly ionized at low altitude, which implies a strong influence from neutrals through collision processes on the EPB motion. This leads to a different regime where friction between neutrals and ions plays a primary role on RTI contrary to the classical case of the collisionless regime. Nonlinear models have already been developed to study the growth of EPB [24,25], but they used a different method which does not take into account the temporal evolution of the bubble shape in addition to its nonlinear growth.

Our primary goal is to determine GRTI nonlinear rising velocity by applying Layzer's approach. We choose to use the extended version proposed by Goncharov [13] to obtain results at an arbitrary Atwood number. Although this model has shown limitations as demonstrated by the work of Mikaelian [26], it has proven to have the best prediction of bubble terminal velocities compared to simulations [27,28] and experiments [29] so far (among Abharzhi's model and Sohn's model). This model could also have some bearing for other fields of application like astrophysics since it depicts a nonlinear RTI process for partially ionized plasma in the limit of very low degree of ionization [30]. This paper is organized as follows. In Sec. II we investigate the nonlinear theory of the GRTI bubble for a plasma in a moving neutral background for a single mode in plane geometry. In Sec. III we compare and discuss the bubble nonlinear model with direct numerical simulations. The specific case of the RTI spike is also examined. Finally our conclusion is given in Sec. IV.

II. NONLINEAR SYSTEM DERIVATION

Our coordinate system is defined as follows: $\mathbf{e}_z$ is the unit vector along the magnetic field **B**, and $\mathbf{e}_x$, $\mathbf{e}_y$ being the transverse coordinates (see Fig. 1). The initial state is given by two

---

*quentin.cauvet@cea.fr

†benoit.bernecker@cea.fr; also at Université Paris–Saclay, CEA, Laboratoire Matière en Conditions Extrêmes (LMCE), 91680 Bruyères-le-Châtel, France.

‡Also at Université Paris–Saclay, CEA, Laboratoire Matière en Conditions Extrêmes (LMCE), 91680 Bruyères-le-Châtel, France and LUTH, Observatoire de Paris, PSL Research University, CNRS, Université Paris Diderot, Sorbonne Paris Cité, 92190 Meudon, France.

§Also at Université Paris–Saclay, CEA, Laboratoire Matière en Conditions Extrêmes (LMCE), 91680 Bruyères-le-Châtel, France.
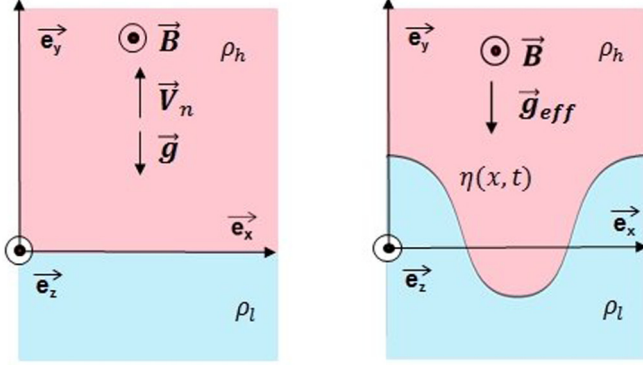
FIG. 1. Geometry of the unperturbed (left) and perturbed (right) states.

plasma fluids separated by an undisturbed plane interface at $y = 0$, with the heavier fluid (with mass density ρ_h) occupying the $y > 0$ region and the lighter fluid (with mass density ρ_l) occupying the $y < 0$ region, and, as a consequence, the magnetic field is taken parallel to the interface. Moreover the system is supposed to be invariant by translation along the z axis (2D geometry).

The two plasma fluids are subject to a gravitational acceleration field taken as $\mathbf{g} = -g\mathbf{e}_y$ (where $g = |\mathbf{g}|$) and to a friction drag force—per unit volume—with a neutral fluid defined as $\mathbf{F}_{h(l)}^n = \rho_{h(l)} \nu_{in}(\mathbf{V}_n - \mathbf{V}_{h(l)})$, where ν_{in} is the momentum exchange collision frequency between ions and neutrals, and $\mathbf{V}_n$ is the velocity of neutrals and is assumed to be constant with $\mathbf{V}_n = U_0\mathbf{e}_y$ (U_0 is either negative or positive). Initially, the two fluids are supposed at hydrostatic equilibrium so that $\mathbf{V}_{h(l)} = 0$. Dynamical equilibrium $\mathbf{V}_{h(l)} = \mathbf{V}_n$ could also be considered without lack of generality. Nevertheless, such an approach would miss the important contribution of GDI in destabilization processes, in the case, for instance, of the ionosphere. Indeed, in the case of $g = 0$ the interface can still be destabilized by GDI process if $\mathbf{V}_{h(l)} \neq \mathbf{V}_n$, but $\mathbf{V}_{h(l)} = \mathbf{V}_n$ will not produce any structures. Note that in the right panel of Fig. 1, $\mathbf{g}$ has been replaced with $\mathbf{g}_{\text{eff}}$. This new acceleration accounts for the combination of the gravitational force and the friction force, $g_{\text{eff}} = g - \nu_{\text{in}}U_0$ (see below).

In the 2D plane approach, the magnetic field is given by

$$\begin{aligned} \mathbf{B} &= B_l(x, y, t)\mathbf{e}_z, \quad y < 0, \\ &= B_h(x, y, t)\mathbf{e}_z, \quad y > 0. \end{aligned} \quad (1)$$

In general, we assume $\mathbf{B}_l \neq \mathbf{B}_h$ at $y = 0$, and, as a consequence a discontinuity for $\mathbf{B}$ takes place at the interface. Since the z component of $\mathbf{B}$ does not depend upon the variable z, the condition $\nabla \cdot \mathbf{B} = 0$ is always satisfied.

We consider a single-mode perturbation of wave number k at the interface, and from this unstable configuration a bubble and a spike grow in the nonlinear regime by RTI processes:

a bubble of light fluid rises in the heavy fluid, and a spike of heavy fluid falls into the light fluid. This behavior is depicted in the right panel of Fig. 1, and the equation of the perturbed interface is $y = \eta(x, t)$.

Our nonlinear study follows the work done by Gupta and his collaborators [31] and by Khan and his collaborators [32] on the nonlinear RTI, which itself follows the initial approach developed by Layzer [10] and improved later by Goncharov [13]. Mitra and his colleagues [33] have even included compressibility effects, but since equatorial ionospheric phenomena are unlikely to involve compressible flows, we have performed our study under the hypothesis of an incompressible fluid, as Gupta *et al.* [31] did previously.

We consider that the top of the bubble (resp. tip of the spike) is located at $x = 0$ and that the bubble (resp. spike) evolves with a parabolic form,

$$\eta(x, t) = \eta_0(t) + \eta_2(t)x^2, \quad (2)$$

where η_0 corresponds to the elevation along y axis of the top (resp. the position of the tip) of a bubble (resp. of a spike); η_0 is positive for a bubble and η_0 is negative for a spike. The quantity η_2 corresponds to the half value of the curvature of the top of a bubble ($\eta_2 < 0$) or the tip of a jet ($\eta_2 > 0$). Equation (2) is a perturbative expression in x of the bubble (resp. spike) shape at the second order [neglecting terms greater than $O(x^i)(i \geqslant 3)$] [31].

Moreover, according to Layzer's approach [10], we suppose that the fluids are incompressible ($\nabla \cdot \mathbf{V} = 0$) and have an irrotational motion, so that the velocity derives from a potential ϕ such as $\mathbf{V} = -\nabla\phi$. The velocity potential for the heavier and lighter fluids obeying the Laplacian equation is assumed to be given by [31]

$$\phi_h(x, y, t) = a_1(t)\cos(kx)e^{-k(y-\eta_0(t))}, \quad y > 0,$$

$$\phi_l(x, y, t) = b_0(t)y + b_1(t)\cos(kx)e^{k(y-\eta_0(t))}, \quad y < 0, \quad (3)$$

with

$$\mathbf{V}_{h(l)} = -\nabla\phi_{h(l)}, \quad (4)$$

where k is the wave number of the perturbation, and the functions $a_1(t)$, $b_0(t)$, and $b_1(t)$, will be determined later [31]. The velocity potential presented here is a local solution at the interface vicinity. It is well known that such an expression [$b_0(t)y$] cannot match the boundary condition at $y \to -\infty$ as previously pointed out by Goncharov [13]. Indeed, this term [$b_0(t)y$] should be multiplied by a slowly decreasing function, but it would only make computation more cumbersome and the use of perturbation series necessary without modifying the solution at interface vicinity. Moreover, direct numerical simulations [27,28] have shown better agreement with Goncharov's model than with others (Abarzhi's model [15] and Sohn's model [14]), satisfying in this way our previous approximation.

The fluid motion is governed by the momentum conservation equation:

$$\rho_{h(l)}\left[\frac{\partial\mathbf{V}_{h(l)}}{\partial t} + (\mathbf{V}_{h(l)} \cdot \nabla)\mathbf{V}_{h(l)}\right] = -\nabla p_{h(l)} + \rho_{h(l)}\mathbf{g} + \rho_{h(l)}\nu_{\text{in}}(\mathbf{V}_n - \mathbf{V}_{h(l)}) + \frac{1}{\mu_{h(l)}}(\nabla \times \mathbf{B}_{h(l)}) \times \mathbf{B}_{h(l)}, \quad (5)$$

where $\mu_{h(l)}$ is the permeability of the fluid and $p_{h(l)}$ is the fluid pressure.

The Lorentz $\mathbf{J} \times \mathbf{B}$ force can be rewritten as

$$\frac{1}{\mu_{h(l)}}(\mathbf{\nabla} \times \mathbf{B}_{h(l)}) \times \mathbf{B}_{h(l)} = \frac{1}{\mu_{h(l)}}(\mathbf{B}_{h(l)} \cdot \mathbf{\nabla})\mathbf{B}_{h(l)} - \frac{1}{2\mu_{h(l)}}\nabla \mathbf{B}_{h(l)}^2, \tag{6}$$

where the first term on the right-hand side refers to the magnetic tension force (which is zero in our case, since the magnetic field is invariant along $\mathbf{e}_z$) and the second term refers to the magnetic pressure force. Using Eq. (4) in (5) for the heavier and lighter fluids one obtains the following Bernoulli's equation:

$$\rho_h\left[-\frac{\partial \phi_h}{\partial t} + \frac{1}{2}(\nabla \phi_h)^2\right] - \rho_l\left[-\frac{\partial \phi_l}{\partial t} + \frac{1}{2}(\nabla \phi_l)^2\right]$$

$$= -g_{\text{eff}}(\rho_h - \rho_l)y + \nu_{\text{in}}(\rho_h\phi_h - \rho_l\phi_l) - (p_h - p_l) - \left(\frac{B_h^2}{2\mu_h} - \frac{B_l^2}{2\mu_l}\right) + f_h(t) - f_l(t), \tag{7}$$

where $g_{\text{eff}} = -\nu_{\text{in}}U_0 + g$ is the effective acceleration field and $f_{h(l)}(t)$ is an arbitrary function of time, which we will not need to determine in our studies. To trigger the GRTI, $g_{\text{eff}} > 0$ is required, and we conclude that a downward, $U_0 < 0$ (resp. upward, $U_0 > 0$) neutral wind will contribute to destabilize (resp. stabilize) the interface.

By balancing the total pressure defined as $p_{t,h(l)} = p_{h(l)} + B_{h(l)}^2/(2\mu_{h(l)})$ on the two sides of the interface, Eq. (7) is much simplified, and it reduces to

$$\rho_h\left[-\frac{\partial \phi_h}{\partial t} + \frac{1}{2}(\nabla \phi_h)^2\right] - \rho_l\left[-\frac{\partial \phi_l}{\partial t} + \frac{1}{2}(\nabla \phi_l)^2\right]$$

$$= -g_{\text{eff}}(\rho_h - \rho_l)y + \nu_{\text{in}}(\rho_h\phi_h - \rho_l\phi_l) + f_h(t) - f_l(t). \tag{8}$$

This equation differs from the equation derived by Gupta *et al.* [31]. These authors do not consider the total magnetic field for the pressure continuity equation. In our view, this assumption, however, is not correct because the only way to avoid the formation of a shock wave at the interface consists in requesting continuity of the total pressure through the interface. Moreover, in our case, the magnetic field does not play a role in RTI formation, since there is not any magnetic tension, which agrees with linear [4] and weakly nonlinear theories [34]. Therefore, our approach seems correct with our knowledge of the magnetized RTI.

The kinematical boundary conditions satisfied at the interface surface $y = \eta(x, t)$ are

$$\frac{\partial \eta}{\partial t} - \frac{\partial \phi_h}{\partial x}\frac{\partial \eta}{\partial x} = -\frac{\partial \phi_h}{\partial y}, \tag{9a}$$

$$\left(\frac{\partial \phi_h}{\partial x} - \frac{\partial \phi_l}{\partial x}\right)\frac{\partial \eta}{\partial x} = \frac{\partial \phi_h}{\partial y} - \frac{\partial \phi_l}{\partial y}. \tag{9b}$$

Finally by substituting in these equations the expression of η from (2) and the expression of $\phi_{h(l)}$ from (3), one obtains the following two ordinary differential equations [31]:

$$\frac{d\xi_1}{d\tau} = \xi_3, \tag{10}$$

$$\frac{d\xi_2}{d\tau} = -\frac{1}{2}(6\xi_2 + 1)\xi_3, \tag{11}$$

$$b_0 = -\frac{6\xi_2}{3\xi_2 - 1/2}\,ka_1, \tag{12}$$

$$b_1 = \frac{3\xi_2 + 1/2}{3\xi_2 - 1/2}\,a_1, \tag{13}$$

where

$$\xi_1 = k\eta_0,$$
$$\xi_2 = \eta_2/k,$$
$$\xi_3 = k^2 a_1/\sqrt{kg_{\text{eff}}},$$
$$\tau = t\sqrt{kg_{\text{eff}}}. \tag{14}$$

In these equations, ξ_1, ξ_2, and ξ_3 are, respectively, the dimensionless (with respect to the wave number and the effective acceleration field) displacement, curvature, and velocity of the top of the bubble (resp. the tip of the spike) and τ is the dimensionless time.

At this step, three unknowns, namely, ξ_1, ξ_2, and ξ_3, have been introduced and only two differential equations have been derived. The third equation governing the variable ξ_3 can be obtained by doing the same in Bernoulli equation (8) and equating the coefficient of x^2 on both sides. We obtain Eq. (15), which completes the set of equations describing the perturbation in its nonlinear regime [with (10) and (11)]:

$$\frac{d\xi_3}{d\tau} = -\frac{6\xi_2 - 1}{D(\xi_2, r)}\left\{\frac{N(\xi_2, r)\xi_3^2}{(6\xi_2 - 1)^2} - 2(r - 1)\xi_2 \right.$$

$$\left. - C\xi_3\left[r(2\xi_2 + 1) - \frac{24\xi_2^2}{6\xi_2 - 1} + (2\xi_2 - 1)\frac{6\xi_2 + 1}{6\xi_2 - 1}\right]\right\}, \tag{15}$$

where

$$r = \rho_h/\rho_l,$$
$$C = \nu_{\text{in}}/\sqrt{kg_{\text{eff}}},$$
$$D(\xi_2, r) = 12(1 - r)\xi_2^2 + 4(r - 1)\xi_2 + (r + 1),$$
$$N(\xi_2, r) = 36(1 - r)\xi_2^2 + 12(4 + r)\xi_2 + (7 - r), \tag{16}$$

where r is the ratio of the mass densities and C is a dimensionless parameter representing the collision drag over gravitational force. The above set of three differential equations describe the time evolution of the top of the bubble (resp. tip of the spike). Actually, following Goncharov's idea [13], the time evolution of the spike is obtained from the same

set by making the transformation $\xi_1 \to -\xi_1$, $\xi_2 \to -\xi_2$, $r \to 1/r$, and $g_{\text{eff}} \to -g_{\text{eff}}$.

This set of equations is valid only in the case $g_{\text{eff}} > 0$. For the case $g_{\text{eff}} < 0$, the dimensionless velocity, time, and parameter C become, $\xi_3 = k^2 a_1/\sqrt{-kg_{\text{eff}}}$, $\tau = t/\sqrt{-kg_{\text{eff}}}$, and $C = v_{\text{in}}/\sqrt{-kg_{\text{eff}}}$. The only other modification is the sign of the second term in the brackets of Eq. (15). This case is easily demonstrated to be stable for the GRTI, and when $\tau \to +\infty$, we have $\xi_2 \to 0$ and $\xi_3 \to 0$.

Equation (15) corresponds to an extension of the studies done by Goncharov [13] and by Gupta *et al.* [31]. The difference with our analysis comes from the additional contribution of the collisions with neutral flow to the RTI. By setting $g_{\text{eff}} = g$ and $C = 0$ in (15), we recover the equation derived by Goncharov [13]. However, our approach does not recover fully the results of Gupta *et al.* [31] mainly due to differences in treatment of the total pressure continuity through the interface that they do not conserve.

It is worth noting that we can rewrite Eq. (15) using the standard Atwood number, $A_t = (\rho_h - \rho_l)/(\rho_h + \rho_l)$, using the transformation $r = (1 + A_t)/(1 - A_t)$.

Finally, let us address the physical interpretation of the dimensionless number C, where v_{in} appears both in the numerator and the denominator. Two limit cases can be obtained according to the values of v_{in}, U_0, and g. First, if the condition $| v_{\text{in}}U_0 | \ll g$ is satisfied, then the dimensionless number reduces to $C_1 = v_{\text{in}}/\sqrt{kg}$, which represents the ratio between the collision frequency and the classical RTI growth rate, for $A_t = 1$. Second, for $| v_{\text{in}}U_0 | \gg g$, the dimensionless number is $C_2 = \sqrt{-v_{\text{in}}/(kU_0)}$ (remember that U_0 is destabilizing), which describes the GDI. In our definition, C combines the two independent phenomena, i.e., the RTI and the GDI, in a single one, and C, C_1, and C_2 obey the relationship $1/C^2 = 1/C_1^2 + 1/C_2^2$.

A. Linear approximation

One of the strengths of the Layzer approach is that even if it is used to determine the nonlinear behavior of the Rayleigh-Taylor structure, the linear regime can be retrieved by linearizing the set of equations (10), (11), and (15). By doing so, we can easily obtain a linear temporal ordinary equation for ξ_3:

$$\frac{d^2\xi_3}{d\tau^2} + C\frac{d\xi_3}{d\tau} - \frac{(r-1)}{r+1}\xi_3 = 0. \tag{17}$$

Assuming the dimensionless velocity of the top of the bubble to be of the form $\xi_3 = \xi_3^0 e^{\gamma'\tau}$ and injecting it into Eq. (17), we obtain the dimensionless growth rate [with $A_t = (r-1)/(r+1) = (\rho_h - \rho_l)/(\rho_h + \rho_l)$]:

$$\gamma' = \frac{\sqrt{C^2 + 4A_t} - C}{2}, \tag{18}$$

which yields the dimension grow rate:

$$\gamma = \sqrt{kg_{\text{eff}}}\frac{\sqrt{C^2 + 4A_t} - C}{2}. \tag{19}$$

In the collisionless (inertial) case (meaning $C \ll 1$), we obtain the classical growth rate [35], $\gamma = \sqrt{A_t g_{\text{eff}} k}$ except for the effective gravity. In the collisional regime, we obtain the growth

rate $\gamma = A_t kg_{\text{eff}}/v_{\text{in}}$, which is similar to the one derived in the literature [21,23]. In the two regimes, we retrieve the linear growth rate.

B. Asymptotic bubble velocity

To determine an analytical asymptotic velocity of the top of a bubble, we consider the limit $d\xi_2/d\tau \to 0$ and $d\xi_3/d\tau \to 0$ when $\tau \to \infty$ so that the shape of the bubble is invariant and the top of the bubble moves upward at constant velocity. This leads to a constant dimensionless curvature, $\xi_2 = -1/6$, from Eq. (11). Finally, the dimensionless velocity ξ_3 is a solution of the following second-degree polynomial:

$$3r\xi_3^2 + (1 + 2r)C\xi_3 - (r - 1) = 0, \tag{20}$$

and the solution is

$$\xi_3 = \frac{1 + 2r}{6r}\left[\sqrt{C^2 + 12\frac{r(r-1)}{(1+2r)^2}} - C\right]. \tag{21}$$

The other root is always negative and is not considered since a downward velocity of the bubble remains unphysical in our case. This form is similar to the one obtained by Ott [24], who assumed a circular bubble. But using the model described by Goncharov [13] allows us to describe the temporal evolution of the nonlinear bubble at arbitrary Atwood number and not only the asymptotic case.

Let us examine the asymptotic behavior of the top of the bubble velocity v_b. By construction, one has $v_b = d\eta_0/dt$, and together with (10) and the definition (14) of the dimensionless quantities, one gets $v_b = (\sqrt{g_{\text{eff}}/k})\xi_3$. Thus, the asymptotic expression of the bubble velocity reads as

$$v_b = \frac{v_{\text{in}}}{k}\frac{1 + 2r}{6r}\left[\sqrt{1 + 12\frac{r(r-1)}{C^2(1+2r)^2}} - 1\right]. \tag{22}$$

This quantity does not correspond to the velocity inside the bubble, but the velocity of its tip at $x = 0$ and $y = \eta_0(t)$. This is all the more true considering that we do not verify the boundary condition at infinity (zero velocity) in the light fluid. For the collisional case (meaning $C \gg 1$), we obtain

$$v_b = \frac{g_{\text{eff}}}{v_{\text{in}}}\frac{r - 1}{1 + 2r}. \tag{23}$$

For a light fluid much lighter than the heavy one (the light fluid corresponds almost to vacuum), then $r \to \infty$ and the expression (23) becomes

$$v_b = \frac{g_{\text{eff}}}{2v_{\text{in}}}, \tag{24}$$

which is a form similar to the one described by Ossakow and Chaturvedi [25].

Using the Atwood number $A_t = (\rho_h - \rho_l)/(\rho_h + \rho_l)$ we can put the velocity in the form

$$v_b = \frac{g_{\text{eff}}}{v_{\text{in}}}\frac{2A_t}{3 + A_t}. \tag{25}$$

In contrast in the collisionless (inertial) case (meaning $C \ll 1$), we obtain

$$v_b = \sqrt{\frac{g_{\text{eff}}}{3k}\frac{r(r-1)}{r^2}}, \tag{26}$$

and using the Atwood number and the wavelength $\lambda = 2\pi/k$, (26) transforms into an equation similar to the result deduced by Goncharov [13], but with our effective acceleration field g_{eff} instead of g:

$$v_b = \sqrt{\frac{\lambda g_{\mathrm{eff}}}{6\pi} \frac{2A_t}{1 + A_t}}. \qquad (27)$$

For $r \to \infty$ ($A_t \to 1$) and $g_{\mathrm{eff}} = g$, this equation leads to the well-known formula

$$v_b = \sqrt{\lambda g/(6\pi)} \qquad (28)$$

derived originally by Mikaelian [12] and Zhang [16] independently.

It is worth noticing the differences of the bubble velocity dependency in the wave number k for the to limit cases $C \to \infty$ and $C = 0$. Indeed, in the first case, v_b is not dependent on k, while in the later, $v_b \propto k^{-1/2}$. Thus, in the strongly collisional case, the bubble can evolve with an asymptotic velocity that is always the same whatever its size, similarly to the linear growth rate [21].

C. Asymptotic spike velocity

To apply the same method to the spike, we need to transform $\eta \to -\eta$ and $g_{\mathrm{eff}} \to -g_{\mathrm{eff}}$ and used the velocity potentials $\phi_h(x, y, t) = b_0(t)y + b_1(t)\cos(kx)e^{-k[y-\eta_0(t)]}$ for heavier fluid ($y > 0$) and $\phi_l(x, y, t) = a_1(t)\cos(kx)e^{k[y-\eta_0(t)]}$ for lighter fluid ($y < 0$). This is equivalent to applying the transformation $2(r-1)\xi_2 \to -2(r-1)\xi_2$ where $2(r-1)\xi_2$ is the second term inside the brackets of Eq. (15) and then the transformation $\xi_1 \to -\xi_1$, $\xi_2 \to -\xi_2$, $r \to 1/r$ in Eqs. (10)–(15). To determine the analytical asymptotic velocity, if any, of the spike we assume that when $\tau \to \infty$, $d\xi_2/d\tau \to 0$ and $d\xi_3/d\tau \to 0$ so that the shape of a spike is invariant and that its tip moves downward at constant velocity (only valid in the collisional regime). The solutions of Eqs. (10)–(15) are a constant dimensionless curvature $\xi_2 = 1/6$ and a constant dimensionless velocity:

$$\xi_3 = -\frac{(r+2)}{6}\left[\sqrt{C^2 + 12\frac{r-1}{(r+2)^2}} - C\right]. \qquad (29)$$

The asymptotic expression of the spike velocity reads as

$$v_s = \frac{v_{\mathrm{in}}}{k} \frac{r+2}{6}\left[\sqrt{1 + 12\frac{r-1}{C^2(r+2)^2}} - 1\right]. \qquad (30)$$

For the collisional case, in the asymptotic limit $C \gg 1$, the velocity v_s of the tip of a spike is given by

$$v_s = \frac{g_{\mathrm{eff}}}{v_{\mathrm{in}}} \frac{r-1}{r+2} = \frac{g_{\mathrm{eff}}}{v_{\mathrm{in}}} \frac{2A_t}{3 - A_t}. \qquad (31)$$

This expression is not the same as for the bubbles, and for $A_t \to 1$, we get $v_s \simeq g_{\mathrm{eff}}/v_{\mathrm{in}}$ where the factor 2 in the denominator is missing compared to the expression of v_b.

In contrast, in the collisionless case ($C \ll 1$), we obtain the same result as Goncharov [13]:

$$v_s = \sqrt{\frac{\lambda g_{\mathrm{eff}}}{6\pi}(1 - r)} = \sqrt{\frac{\lambda g_{\mathrm{eff}}}{6\pi} \frac{2A_t}{1 - A_t}}. \qquad (32)$$

The discontinuity in the case A_t is explained by the free falling motion into vacuum [11], $v_s \sim gt$.

Similarly to bubble velocities, spike velocity does not depend on the wave number k for the to limit cases $C \to \infty$ while for $C = 0$, $v_s \propto k^{-1/2}$. Thus, in the strongly collisional case, the bubble can evolve with an asymptotic velocity that is always the same whatever its size is.

III. NUMERICAL SIMULATION

A. Software

To confirm our results, we have performed simulations using two codes: CLOVIS and ERINNA. Based on the hierarchy defined by Besse and his coauthors [36], the ideal magnetohydrodynamics (MHD) model (collisionless and collisional regimes) is solved with CLOVIS and the striation model (only collisional regime) with ERINNA. These two approaches permit us to examine the transition between the results of the collisionless and collisional regimes of the GRTI with CLOVIS and the results in the fully collisional regime with ERINNA.

1. CLOVIS

CLOVIS [37,38] is a three-dimensional (3D) Godunov-type code that resolves on an Eulerian fixed Cartesian mesh with HLLD [39] or Roe [40] Riemann solvers the ideal MHD equations written in their conservative form:

$$\frac{\partial \rho}{\partial t} + \nabla \cdot [\rho \mathbf{V}] = 0, \qquad (33a)$$

$$\frac{\partial (\rho \mathbf{V})}{\partial t} + \nabla \cdot [\rho \mathbf{V} \otimes \mathbf{V} - \mathbf{B} \otimes \mathbf{B} + p_t \mathbf{I}] = \mathbf{S}^I, \qquad (33b)$$

$$\frac{\partial \mathcal{E}}{\partial t} + \nabla \cdot [(\mathcal{E} + p_t)\mathbf{V} - (\mathbf{V} \cdot \mathbf{B})\mathbf{B}] = S^{II}, \qquad (33c)$$

$$\frac{\partial \mathbf{B}}{\partial t} + \nabla \cdot [\mathbf{V} \otimes \mathbf{B} - \mathbf{B} \otimes \mathbf{V}] = 0, \qquad (33d)$$

where the symbol $\otimes$ stands for the tensor product and where $\mathcal{E}$ is the total energy density, and $\mathbf{S}^I$ and S^{II} are the source terms due to friction and gravity in momentum and energy conservation equations, respectively. $\mathbf{S}^I = \rho \mathbf{g} + \rho v_{\mathrm{in}}(\mathbf{V}_n - \mathbf{V})$, as expected from Eq. (5). For S^{II}, the source term for gravity is $\rho \mathbf{V} \cdot \mathbf{g}$, and for the friction drag with neutral, we assume adiabatic collision. Notice that for numerical reasons the magnetic field in CLOVIS is normalized by the factor $1/\sqrt{\mu_0}$. Due to these contributions, CLOVIS is able to compute various configurations where the value of C is a tunable parameter.

2. ERINNA

ERINNA [41] is a two-dimensional (2D) Eulerian code that solves the convection-diffusion and elliptic equations:

$$\frac{\partial \rho}{\partial t} - \frac{1}{B}\nabla \cdot (\rho \nabla_\perp \phi_E) - \kappa \Delta \rho = 0, \qquad (34a)$$

$$-\frac{1}{B}\nabla \cdot (\rho \nabla \phi_E) + \nabla \cdot (\rho \mathbf{V}_n \times \mathbf{e}_z) = 0, \qquad (34b)$$

where $\nabla_\perp = (-\partial_y, \partial_x)$, ϕ_E is the electric potential defined by $\mathbf{E} = -\nabla\phi_E$ with $\mathbf{E}$ the electric field following Ohm's law $\mathbf{E} = -\mathbf{V} \times \mathbf{B}$, and κ is a diffusion coefficient. This

coefficient is required to prevent the cascading of our single mode into smaller ones [21]; see below. Moreover, ERINNA is restricted to simulations of highly collisional configurations ($C \gg 1$). This property will be useful to study the limit case $C \to \infty$.

One may notice that ν_{in} is missing in the equation solved with ERINNA; this is merely due to the fact that in reality it multiplies all the Eqs. (34b), and it can be canceled without any effect on our solution. Similarly, B will merely affect the numerical value of ϕ_E without changing the dynamics of our situation. Moreover in this striation model gravity is not present so that g_{eff} reduces to $\nu_{in} U_0$ and the top of the bubble (resp. tip of the spike) velocity is proportional to U_0.

B. Initialization

1. CLOVIS

CLOVIS, as an MHD algorithm, allows us to observe the effect of the parameter C on the terminal velocity of the RTI structure. The domain is defined by $x \in [-1; 1]$ m and $y \in [-12; 12]$ m with a resolution of 300×50. Periodic boundary conditions in the lateral directions and wall boundary conditions in the direction of gravity were used. The density of the light fluid is $\rho_l = 1$ kg m^{-3}. The ambient pressure field is $p_0 = 100$ Pa for $A_t = 1/3$ and $p_0 = 200$ Pa for $A_t = 9/11$. The ambient magnetic field is $B_0 = 100$ Pa$^{1/2}$. Notice that in CLOVIS the magnetic field as been normalized to $\sqrt{\mu_0}$ so that the magnetic pressure can be written as $\mathbf{B}^2$. This configuration is used to verify the incompressibility condition $|\mathbf{V}_{h(l)}| \ll C_s$, where C_s is the sound velocity, which was required since CLOVIS is a compressible code. Furthermore, in order to be entirely consistent with ionospheric conditions, we verified $C_s \ll V_a$, where V_a is the Alfvén velocity. A gravitational field of intensity $g = 1$ m s^{-2} is exerted on the two fluids. The neutral are supposed at rest so that $g_{eff} = g$. Finally, we adjust the collisional frequency ($\nu_{in} \in [0.7, 1, 2, 3, 5, 7, 10, 20, 30]$ s^{-1}) to see its impact on the terminal velocity of RTI structure. We perturb our equilibrium state with the velocity field:

$$v_{y0} = \alpha[1 + \cos(kx)]\cos(3ky/4), \quad (35)$$

where α is the initial amplitude.

2. ERINNA

The domain is defined by $x \in [0, 12\,000]$ m and $y \in [0, 12\,000]$ m. The density of the light fluid is $\rho_l = 1$ kg m^{-3} for $y > 6000$ m and ρ_h varied for $y < 6000$ m. A neutral wind is added as $\mathbf{V}_n = U_0 \mathbf{e}_y$ with $U_0 = 100$ m s^{-1}. The boundary condition is $\phi_E = 0$ at $x = 0$ or $x = 12\,000$ m and $\nabla \phi_E = 0$ V at $y = 0$ and $y = 12\,000$ m. Due to the lack of a periodic condition in this code, we initialize an array of bubbles or jets to compensate for the boundary effect. The wavelength is $\lambda = 1500$ m between $x \in [1500; 10\,500]$ m resulting in seven bubbles or jets, allowing us to ignore the border effect by measuring the growth rate of the central one. This time the perturbation is applied to the ion density:

$$\rho(x, y) = \rho_s\{1 \pm \alpha \cos[k(x - x_0)]\}, \quad (36)$$

where $\alpha = 0.01$, $s \in h, l$, $x_0 = 6000$ m, and the perturbation is negative for a bubble and positive for a spike. The advantage
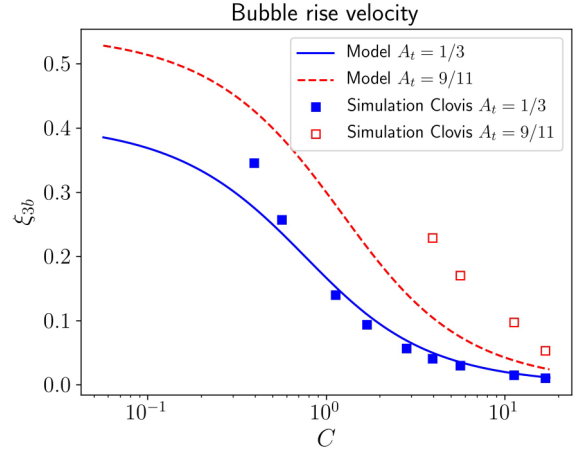

FIG. 2. Comparison of the asymptotic velocity of the top of the bubble as a function of the collision parameter calculated with our model and CLOVIS for $A_t = 1/3$ ($r = 2$), (solid blue line and filled squares) and $A_t = 9/11$ ($r = 10$) (dashed red line and emptied squares).

of ERINNA over CLOVIS is that it allows for fully collisional simulation at a far lower computing cost. Nonetheless, new issues emerge, such as the bifurcation of our instability structure onto a smaller scale [21]. To prevent our bubble or jet array from bifurcating, we must include an artificial diffusion in the conservation density equation (34a). As previously stated, when the density ratio is larger, a higher diffusion is required to maintain a jet unity [42]; therefore we modify κ as consequence ($\kappa = 100$ m^2 s^{-1} for $\rho_h \in [1.25, 1.5, 2]$ kg m^{-3}, $\kappa = 200$ m^2 s^{-1} for $\rho_h \in [3, 5]$ kg m^{-3} and $\kappa = 600$ m^2 s^{-1} for $\rho_h \in [7, 10, 20]$ kg m^{-3}). In our simulation, $B = 500$ nT.

C. Application to bubble

In this section, numerical simulations with CLOVIS and ERINNA are performed, and the results are compared to those derived from our analytical model.

1. Results

Figure 2 compares the calculations obtained with CLOVIS to the analytical results for the variation of the bubble normalized velocity ξ_{3b} as a function of the collision parameter C using Eq. (21) for a fluid interface with $A_t = 1/3$ ($r = 2$) and $A_t = 9/11$ ($r = 10$). For large values of C, Eq. (23) shows that $\xi_{3b} \sim 1/C$, and this behavior is clearly recovered for $A_t = 1/3$ with a good agreement between simulations and theory. The same variation takes place for $A_t = 9/11$; however, the numerical values of the velocity are about twice larger than the analytical ones. We believe this discrepancy originates in the value of the Atwood number close to unity; see Fig. 3 and Table I.

In what follows, we restrict ourselves to the strongly collisional case ($C \gg 1$), and, as a consequence, our analytical model is compared to numerical simulations achieved with ERINNA. In Fig. 3 the terminal velocity of the top of a bubble is plotted in terms of A_t. Actually, we plot the parameter α defined according to the relation $v_b = \alpha g_{eff}/\nu_{in}$. At this stage we focus on the black curve (labeled $n = 1$, where n is the order
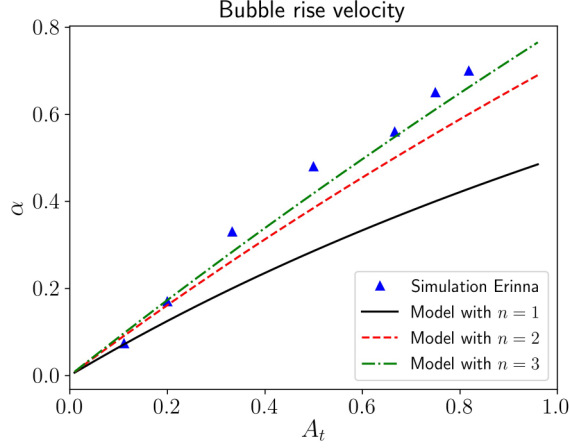
FIG. 3. Comparison of the asymptotic velocity of the top of the bubble as a function of Atwood number calculated by our model (solid, dashed, and dotted-dashed lines for $n = 1$, $n = 2$, and $n = 3$, respectively) and ERINNA (triangles).

of the expansion; see below for the significance of the index n) and as expected from Eq. (24), we get $\alpha = 1/2$ for $A_t = 1$. For $A_t < 0.2$, the agreement between ERINNA and the analytical model is not bad, but for $A_t > 0.5$, the numerical values are about twice larger than the theoretical ones and, especially, $\alpha \simeq 1$ for $A_t = 1$. This discrepancy is an interesting issue, and in the next section we extend the model in order to improve the agreement between simulations and theory. Furthermore, it is well known that in the collisionless regime, the potential flow model exhibits some limitation [26]. This question will also be addressed, and the difference between the collisional and the collisionless cases will be highlighted.

2. Discussion

In the collisionless regime the irrotational motion assumption (also known as potential flow) is not well satisfied at low Atwood number. In previous works it has been shown that bubble terminal velocity is maintained only for a transient time due to vorticity which reaccelerates the bubble [43]. Using Layzer's method, Betti and Sanz [44] have improved Goncharov's work by including the effect of vorticity in the bubble asymptotic velocity. This is done by considering a rotational flow in the light fluid with vorticity $\nabla \times \mathbf{V}_l = \omega \mathbf{e}_z$. The authors use a stream function Ψ ($\mathbf{V}_l = \nabla \psi \times \mathbf{e}_z$), which satisfies $\Delta \Psi = -\omega$, and taking the simple ansatz $\omega = -\omega_0(t) \sin(kx)$ for the vorticity, the stream function can be

TABLE I. Result of the nonlinear equation of the bubble terminal velocity in the collisional regime for $A_t = 1$ using *Mathematica* software.

Expansion to order x^{2n}	α such as $v_b = \alpha g_{\mathrm{eff}}/\nu_{\mathrm{in}}$	ξ_2
$n = 1$	0.500	−0.16666
$n = 2$	0.714	−0.2500
$n = 3$	0.793	−0.27346
$n = 4$	0.843	−0.30098

written as

$$\Psi(x, y, t) = -b_0(t)x + \left[b_1(t)e^{k(y-\eta_0(t))} + \frac{\omega_0(t)}{k^2} \right] \sin(kx),$$

(37)

which is equivalent to $\mathbf{V}_l = -\nabla \phi_l + \nabla \chi \times \mathbf{e}_z$ with $\chi = (\omega_0/k^2) \sin(kx)$ [45–47]. The asymptotic bubble velocity then become [44]

$$v_b^{rot} \approx \sqrt{\frac{g}{3k} \frac{r(r-1)}{r^2} + \frac{1}{r} \frac{\omega_0^2}{4k^2}}.$$

(38)

This approach has recently shown promising results to explain the discrepancy between Goncharov model and simulations at low Atwood number [48]. It may also explain why there was no evident saturation in our simulation when $C < 1$ as seen in Fig. 2.

This problem cannot arise in the collisional regime. Indeed, in this case the vorticity obeys the following equation:

$$\frac{\partial \omega}{\partial t} + \mathbf{V}_l \cdot \nabla \omega = -\nu_{\mathrm{in}}\omega,$$

(39)

and its solution shows that the vorticity decays exponentially with time along stream lines [24]. This property associated with our simulation results shows that the potential flow model developed by Goncharov is appropriate to describe the nonlinear regime of the collisional limit of the GRTI. Yet our present purpose is improving the agreement between theory and ERINNA simulations as pointed out in the previous section about Fig. 3.

In the original paper by Layzer [10], only the first harmonic was used and Goncharov has shown that higher harmonic contributions can be neglected in the collisionless regime [13].

Some earlier attempts in the case of Atwood number equal to unity ($A_t = 1$) have been performed to derive an exact solution for the flow by using velocity potential near the top of the bubble decomposed in a Fourier series according to [49,50]

$$\phi = \sum_{j=1}^{+\infty} a_j e^{jk(ix-y)}.$$

(40)

To avoid imaginary solutions, we follow the approach by Goncharov by taking into account the odd modes only of the Fourier series [13]:

$$\phi_h = \sum_{j=0}^{+\infty} a_{2j+1} \cos[(2j+1)kx] e^{-(2j+1)k(y-\eta_0)},$$

(41)

$$\phi_l = \sum_{j=0}^{+\infty} b_{2j+1} \cos[(2j+1)kx] e^{(2j+1)k(y-\eta_0)} + b_0 y,$$

(42)

and accordingly the interface follows the expansion

$$\eta(x, t) = \sum_{j=0}^{+\infty} \eta_{2j} x^{2j}.$$

(43)

We solve equations (8) and (9) for $A_t = 1$ ($r \to \infty$) in the collisional regime in order to derive the nonlinear bubble saturation velocity. In that case, the Bernouilli equation (8) takes the especially simple form $-g_{\mathrm{eff}} \rho_h y + \nu_{\mathrm{in}} \phi_h + f_h(t) = 0$, which is equivalent to the elliptic equation (34b) used with

ERINNA. This approximation holds because $C \gg 1$ meaning that $1/\sqrt{C} = 1/(\sqrt{kg_{\text{eff}}}\, v_{\text{in}}) \ll 1$, which represents the dimensionless mean time between ion and neutral collisions (see the hierarchy defined by Besse and his coauthors [36] for further explanation). Using then the expression (41) for ϕ_h and (43) for η, the expansion of the equations to order x^{2n}, i.e., only the coefficients a_{2j+1} with $j \leqslant n-1$ are kept nonzero, provides the coefficient α (still defined by $v_b = \alpha g_{\text{eff}}/v_{\text{in}}$). Equation (24) shows that $\alpha = 1/2$ for $n = 1$, and we have seen that the dimensionless curvature is $\xi_2 = 1/6 = 0.16666$. These values are reported in Table I together with the values derived for $n = 2$, $n = 3$ and $n = 4$.

It is seen that the impact of high harmonics cannot be neglected in the collisional regime of the GRTI contrary to the classical RTI, i.e., the collisionless GRTI. The terminal velocity of the top of the bubble clearly increases when adding higher frequency terms on the one hand, and the bubble curvature decreases which gives a sharper shape of the bubble on the other hand. It is instructive to notice that for $n = 4$ (expansion up to x^8), we have $\alpha \approx 0.85$, which agrees rather well with the extrapolation of the values obtained with ERINNA (blue triangles in Fig. 3) for $A_t = 1$.

Additionally, we have solved Eqs. (8) and (9) at arbitrary Atwood number up to order $n = 3$. The results have been plotted in Fig. 3: the dashed red line for $n = 2$ and dotted-dashed green line for $n = 3$. It turns out that the accordance between simulations and theory increases for increasing order, and for $n = 3$ a good agreement between the numerical and the analytical results is observed.

One could have predicted that high harmonics are more important in the collisional regime since it is well known that plasma bubbles bifurcate [51], i.e., a bubble splits into two smaller bubbles, while in the classical case, it is rather a merging process [52] (two neighboring bubbles fuse into a bigger one). Bifurcations have been studied numerically [21,42], and it has been observed that the splitting is strongly dependent on the value of the diffusion coefficient κ. They have found that the larger κ is, the later bifurcations take place. As a consequence, if we want our numerical simulations with ERINNA to be consistent with the single-mode potential model, the value of κ should be large enough to prevent the formation of bubbles at smaller scale. Actually, for an Atwood number near unity, the diffusion coefficient has been adjusted in such a way that the characteristic diffusion time $t_c^n = (\lambda_n)^2/\kappa$ for the fourth harmonics ($n = 4$ and $\lambda_n = 2\pi/[(2n+1)k]$) is of the same order of magnitude as the computational time of our simulations with ERINNA. This condition implies that harmonics up to $n = 3$ do not bifurcate, and for this reason the theoretical curve $n = 4$ has not been computed in Fig. 3.

We conclude that even though the elementary model with Eqs. (3) gives a good order of magnitude of the velocity of the bubble, it underestimates v_b by a factor of two roughly. This shortcoming can be removed by taking into account the harmonics in the model; the price to pay is the more complex computations.

D. Application to spikes

In Sec. II it was outlined that the model is applicable to spikes. This is inspired by the previous studies by Zhang
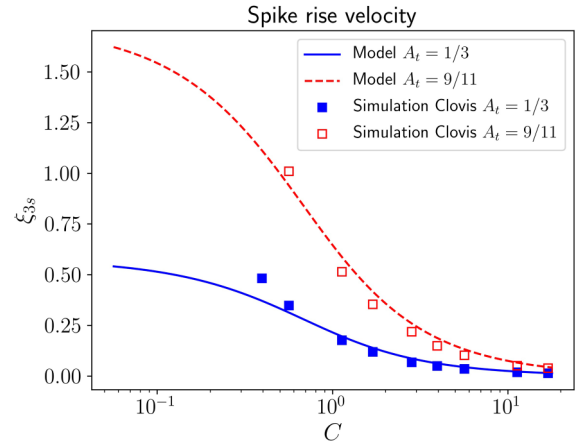
FIG. 4. Comparison of the asymptotic velocity of the tip of a spike as a function of the collision parameter calculated by our model and CLOVIS for $A_t = 1/3$ ($r = 2$), (solid blue line and blue squares) and $A_t = 9/11$ ($r = 10$) (dashed red line and open red squares).

(for $A_t = 1$) [11] and Goncharov (for arbitrary Atwood number) [13] where nonlinear models for the classical RTI spikes are proposed. Although the work by Zhang [11] seems quite successful as it gives a free-fall motion of the spike, generally speaking spike modeling is rarely in agreement with simulations and experiments unlike to bubble models. Indeed, as pointed out by the author and outlined by Mikaelian [26], the Goncharov model [13] fails most of the time. For $A_t \geqslant 0.1$ numerical simulations do not lead to a constant velocity of spikes as predicted by theory. According to Goncharov, this deviation is due to vorticity, which is not included in his theory. Another missing ingredient is the contribution of the harmonics. He took them into account for bubbles but only a very little effect was observed, and he decided therefore not to include them for the spikes. In 2013, a new model was published by Banerjee and his collaborators [53] where the velocity potential in the spike is changed from the form $\phi_h = b_0(t)y + b_1(t)\cos(kx)e^{ik[y-\eta_0(t)]}$ to $\phi_h = b_1(t)\cos(kx)e^{ik(y-\eta_0(t))} + b_2(t)\cos(2kx)e^{i2k[y-\eta_0(t)]}$; i.e., a dependence in the second harmonic, $2k$, is accounted for. Although the model cannot be solved analytically in contrast to the Goncharov approach, the authors find that (1) the value of the bubble velocity is almost not modified compared to (27) where $g_{\text{eff}} = g$ and (2) the spike experiences a free-fall motion at arbitrary Atwood number. This result shows that by considering the second harmonic we can drastically change the spike behavior while the effect on the bubble is very little.

Now an interesting question arises. In opposition to the classical RTI (collisionless GRTI), we have seen that for the collisional GRTI the motion of bubbles is strongly dependent upon the harmonics. Does the same behavior occur for the spikes?

Results obtained from simulations with CLOVIS are exhibited in Fig. 4 (blue and red open squares) where they are compared to the model (solid blue line and dashed red line). As aforementioned, there was no velocity saturation in the inertial regime ($C \ll 1$) [54]. Similarly to bubbles (Fig. 2) a good agreement between numerical calculations and theory is observed for $A_t = 1/3$. Moreover, and unlike bubbles, the same good agreement occurs for $A_t = 9/11$. This
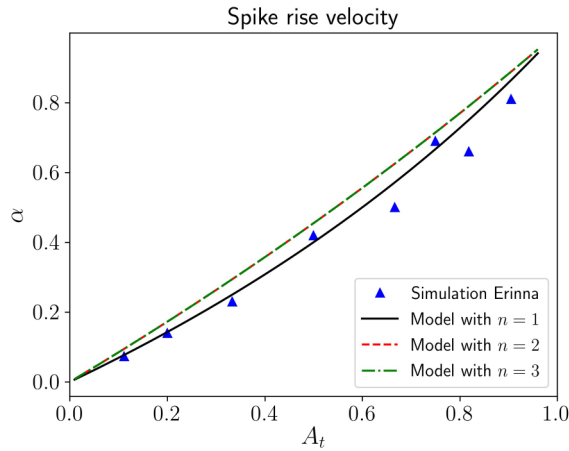
FIG. 5. Comparison of the asymptotic velocity of the tip of a spike as a function of Atwood number calculated by our model (solid, dashed, and dotted-dashed lines for $n = 1$, $n = 2$, and $n = 3$, respectively) and ERINNA (triangles).

unexpected behavior has been checked with the code ERINNA as shown in Fig. 5 where the coefficient α defined according to $v_s = \alpha g_{\mathrm{eff}}/\nu_{\mathrm{in}}$ [see Eq. (31)] is plotted. The blue triangles correspond to the simulations, and they are compared to the analytical results for $n = 1$, $n = 2$, and $n = 3$. Three properties need to be highlighted. First, for $A_t \to 1$, one obtains $\alpha \to 1$ in all cases. This value fully agrees with the analytical formula (31). Second, irrespectively of the value of the index n, the three theoretical curves are almost superimposed, and finally these curves fit pretty well the numerical results. The Layzer model ($n = 1$) is therefore a good approximation for the description of the behavior of the spikes for the collisional GRTI. Although this conclusion is quite opposite to the one deduced for the classical RTI (collisionless GRTI), it could have been expected. Indeed, in the collisional regime, the friction prevents the spikes from entering a free-fall stage and, in addition, since the vorticity decays exponentially, the spikes cannot be reaccelerated by rotational motions. These two combined effects make the analytical results are almost insensitive to the value of n.

IV. CONCLUSION

In this paper, we have studied the non linear evolution of the generalized Rayleigh-Taylor instability (GRTI), i.e., the

Rayleigh-Taylor instability (RTI) arising in a partially ionized, magnetized plasma where the collisions between ions and neutrals are taken into account. For a plasma with very few collisions (collisionless case), the GRTI reduces to the "classical" RTI, while for collision-dominated plasmas (collisional GRTI), the friction between ions and neutrals has significant effects on the dynamics of both the bubbles and the spikes. These effects are examined analytically from an extension of the potential flow model presented by Goncharov [13], and numerically with two dedicated codes, CLOVIS and ERINNA. This model is known to reproduce efficiently the terminal velocity of bubbles in the collisionless GRTI (classical RTI); however, it fails to describe the behavior of spikes mainly due to the missing vorticity in the potential approach. The collisional GRTI leads to an opposite conclusion. Due to the friction, we have shown first that any vorticity contribution decays exponentially and second the spike terminal velocity is a constant. These predictions have been checked numerically, and a good agreement between theory and simulations has been obtained. However, unexpectedly the critical point is regarding the bubbles. Despite the correct order of magnitude of the bubble terminal velocity, the numerical values are about twice larger than the theoretical ones at any Atwood number. Following an idea initially developed by Abarzhi [50] and Inogamov and Abarzhi [49] and used later by Goncharov [13], we have been able to overcome the issue by adding higher harmonics in the velocity potential. With such a correction, the discrepancy for the bubble velocity has been removed, while, interestingly, the spike velocity was mostly kept unchanged. This property is in contrast with the classical RTI case for which Goncharov's model is reliable for bubbles but incorrect for spikes.

Comparisons between the model and experiments or observations remain necessary to validate completely this theoretical work. However, it seems promising to understand geophysical interchange instabilities, and they could have some interest for astrophysical structure formation in the non-linear regime.

Furthermore, in the situation of $A_t \neq 1$, a comparison with alternative models [14–17] would be interesting for further studies to examine if our results are universal or intrinsic to Goncharov's model [13]. Nonetheless, the various models [13–16] converge to the same solution for $A_t = 1$, indicating that our model is reliable in this physical range.

[1] Y. Zhou, Rayleigh–Taylor and Richtmyer–Meshkov instability induced flow, turbulence, and mixing. I, Phys. Rep. **720**, 1 (2017).

[2] Y. Zhou, Rayleigh–Taylor and Richtmyer–Meshkov instability induced flow, turbulence, and mixing. II, Phys. Rep. **723**, 1 (2017).

[3] M. C. Kelley, *The Earth's Ionosphere: Plasma Physics and Electrodynamics* (Academic Press, Singapore, 2009).

[4] S. Chandrasekhar, *Hydrodynamic and Hydromagnetic Stability* (Oxford University Press, Oxford, 1961).

[5] S. Liberatore and S. Bouquet, Analytical modeling of magnetic Rayleigh–Taylor instabilities in compressible fluids, Phys. Fluids **20**, 116101 (2008).

[6] B. Basu, On the linear theory of equatorial plasma instability: Comparison of different descriptions, J. Geophys. Res.: Space Phys. **107**, 18 (2002).

[7] P. Sultan, Linear theory and modeling of the Rayleigh-Taylor instability leading to the occurrence of equatorial spread F, J. Geophys. Res.: Space Phys. **101**, 26875 (1996).

[8] A. J. Díaz, R. Soler, and J. Ballester, Rayleigh-Taylor instability in partially ionized compressible plasmas, Astrophys. J. **754**, 41 (2012).

[9] A. J. Díaz, E. Khomenko, and M. Collados, Rayleigh-Taylor instability in partially ionized compressible plasmas: One fluid approach, Astron. Astrophys. **564**, A97 (2014).

[10] D. Layzer, On the instability of superposed fluids in a gravitational field. Astrophys. J. **122**, 1 (1955).

[11] Q. Zhang, Analytical Solutions of Layzer-Type Approach to Unstable Interfacial Fluid Mixing, Phys. Rev. Lett. **81**, 3391 (1998).

[12] K. O. Mikaelian, Analytic Approach to Nonlinear Rayleigh-Taylor and Richtmyer-Meshkov Instabilities, Phys. Rev. Lett. **80**, 508 (1998).

[13] V. N. Goncharov, Analytical Model of Nonlinear, Single-Mode, Classical Rayleigh-Taylor Instability at Arbitrary Atwood Numbers, Phys. Rev. Lett. **88**, 134502 (2002).

[14] S.-I. Sohn, Simple potential-flow model of Rayleigh-Taylor and Richtmyer-Meshkov instabilities for all density ratios, Phys. Rev. E **67**, 026301 (2003).

[15] S. I. Abarzhi, K. Nishihara, and J. Glimm, Rayleigh–Taylor and Richtmyer–Meshkov instabilities for fluids with a finite density ratio, Phys. Lett. A **317**, 470 (2003).

[16] Q. Zhang and W. Guo, Universality of finger growth in two-dimensional Rayleigh-Taylor and Richtmyer-Meshkov instabilities with all density ratios, J. Fluid Mech. **786**, 47 (2016).

[17] J. A. Zufiria, Bubble competition in Rayleigh–Taylor instability, Phys. Fluids **31**, 440 (1988).

[18] P. Clavin and F. Williams, Asymptotic spike evolution in Rayleigh–Taylor instability, J. Fluid Mech. **525**, 105 (2005).

[19] D. Hysell, An overview and synthesis of plasma irregularities in equatorial spread *F*, J. Atmos. Sol. Terr. Phys. **62**, 1037 (2000).

[20] H. Booker and H. Wells, Scattering of radio waves by the *F*-region of the ionosphere, J. Geophys. Res. **43**, 249 (1938).

[21] C. Besse, J. Claudel, P. Degond, F. Deluzet, G. Gallice, and C. Tessieras, Instability of the ionospheric plasma: Modeling and analysis, SIAM J. Appl. Math. **65**, 2178 (2005).

[22] C. E. Seyler, J. M. Rosado-Román, and D. T. Farley, A non-local theory of the gradient-drift instability in the ionospheric *E*-region plasma at mid-latitudes, J. Atmos. Sol. Terr. Phys. **66**, 1627 (2004).

[23] S. Zargham and C. Seyler, Collisional and inertial dynamics of the ionospheric interchange instability, J. Geophys. Res. **94**, 9009 (1989).

[24] E. Ott, Theory of Rayleigh-Taylor bubbles in the equatorial ionosphere, J. Geophys. Res. **83**, 2066 (1978).

[25] S. L. Ossakow and P. Chaturvedi, Morphological studies of rising equatorial spread *F* bubbles, J. Geophys. Res. **83**, 2085 (1978).

[26] K. O. Mikaelian, Limitations and failures of the Layzer model for hydrodynamic instabilities, Phys. Rev. E **78**, 015303(R) (2008).

[27] G. Dimonte, P. Ramaprabhu, D. Youngs, M. Andrews, and R. Rosner, Recent advances in the turbulent Rayleigh–Taylor instability, Phys. Plasmas **12**, 056301 (2005).

[28] P. Ramaprabhu and G. Dimonte, Single-mode dynamics of the Rayleigh-Taylor instability at any density ratio, Phys. Rev. E **71**, 036314 (2005).

[29] J. Wilkinson and J. Jacobs, Experimental study of the single-mode three-dimensional Rayleigh-Taylor instability, Phys. Fluids **19**, 124102 (2007).

[30] J. L. Ballester, I. Alexeev, M. Collados, T. Downes, R. F. Pfaff, H. Gilbert, M. Khodachenko, E. Khomenko, I. F. Shaikhislamov, R. Soler, *et al.*, Partially ionized plasmas in astrophysics, Space Sci. Rev. **214**, 58 (2018).

[31] M. R. Gupta, L. Mandal, S. Roy, and M. Khan, Effect of magnetic field on temporal development of Rayleigh–Taylor instability induced interfacial nonlinear structure, Phys. Plasmas **17**, 012306 (2010).

[32] M. Khan, L. Mandal, R. Banerjee, S. Roy, and M. Gupta, Development of Richtmyer–Meshkov and Rayleigh–Taylor instability in the presence of magnetic field, Nucl. Instrum. Methods Phys. Res. A **653**, 2 (2011).

[33] A. Mitra, L. Mandal, R. Roychoudhury, and M. Khan, Combined effect of magnetic field and compressibility on Rayleigh-Taylor instability, Open J. Fluid Dynamics **5**, 322 (2015).

[34] D. E. Ruiz, On a variational formulation of the weakly non-linear magnetic Rayleigh–Taylor instability, Phys. Plasmas **27**, 022121 (2020).

[35] Lord Rayleigh, Investigation of the character of the equilibrium of an incompressible heavy fluid of variable density, Proc. London Math. Soc. **s1–14**, 170 (1882).

[36] C. Besse, P. Degond, F. Deluzet, J. Claudel, G. Gallice, and C. Tessieras, A model hierarchy for ionospheric plasma modeling, Math. Models Methods Appl. Sci. **14**, 393 (2004).

[37] Q. Cauvet, Modélisation magnétohydrodynamique, arXiv:2112.08120 (2019).

[38] M. Salmon, Evolution and structuration of diamagnetic cavities in the ionosphere, master's thesis, PFE-Project Graduation, EN-STA, 2021.

[39] T. Miyoshi and K. Kusano, A multi-state HLL approximate Riemann solver for ideal magnetohydrodynamics, J. Comput. Phys. **208**, 315 (2005).

[40] P. L. Roe, Approximate Riemann solvers, parameter vectors, and difference schemes, J. Comput. Phys. **43**, 357 (1981).

[41] F. Hermeline, A finite volume method for the approximation of convection–diffusion equations on general meshes, Int. J. Numerical Meth. Eng. **91**, 1331 (2012).

[42] B. McDonald, S. Ossakow, S. Zalesak, and N. Zabusky, Scale sizes and lifetimes of *F* region plasma cloud striations as determined by the condition of marginal stability, J. Geophys. Res. **86**, 5775 (1981).

[43] P. Ramaprabhu, G. Dimonte, Y.-N. Young, A. C. Calder, and B. Fryxell, Limits of the potential flow approach to the single-mode Rayleigh-Taylor problem, Phys. Rev. E **74**, 066308 (2006).

[44] R. Betti and J. Sanz, Bubble Acceleration in the Ablative Rayleigh-Taylor Instability, Phys. Rev. Lett. **97**, 205002 (2006).

[45] R. Banerjee, L. Mandal, S. Roy, M. Khan, and M. Gupta, Combined effect of viscosity and vorticity on single mode Rayleigh–Taylor instability bubble growth, Phys. Plasmas **18**, 022109 (2011).

[46] R. Banerjee, Combined effect of horizontal magnetic field and vorticity on Rayleigh Taylor instability, arXiv:1608.02072 (2016).

[47] R. Banerjee, Nonlinear Rayleigh–Taylor instability with horizontal magnetic field, Indian J. Phys. **94**, 927 (2020).

[48] X. Bian, H. Aluie, D. Zhao, H. Zhang, and D. Livescu, Revisiting the late-time growth of single-mode Rayleigh–Taylor instability and the role of vorticity, Physica D **403**, 132250 (2020).

[49] N. A. Inogamov and S. I. Abarzhi, Dynamics of fluid surface in multidimension, Physica D **87**, 339 (1995).

[50] S. I. Abarzhi, Nonlinear three-dimensional Rayleigh-Taylor instability, Phys. Rev. E **59**, 1729 (1999).

[51] A. Carrasco, A. Pimenta, C. Wrasse, I. Batista, and H. Takahashi, Why do equatorial plasma bubbles bifurcate? J. Geophys. Res.: Space Phys. **125**, e2020JA028609 (2020), and references therein.

[52] B. Cheng, J. Glimm, and D. Sharp, A three-dimensional renormalization group bubble merger model for Rayleigh–Taylor mixing, Chaos **12**, 267 (2002).

[53] R. Banerjee, L. Mandal, M. Khan, and M. R. Gupta, Spiky development at the interface in Rayleigh-Taylor instability: Layzer approximation with second harmonic, J. Modern Phys. **4**, 174 (2013).

[54] P. Ramaprabhu, G. Dimonte, P. Woodward, C. Fryer, G. Rockefeller, K. Muthuraman, P.-H. Lin, and J. Jayaraj, The late-time dynamics of the single-mode Rayleigh-Taylor instability, Phys. Fluids **24**, 074107 (2012).